



# Highly Angiogenic, Nonthrombogenic Bone Marrow Mononuclear Cell–Derived Spheroids in Intraportal Islet Transplantation

Bae Jun Oh,<sup>1,2</sup> Sang-Man Jin,<sup>1,2</sup> Yoonha Hwang,<sup>3</sup> Jin Myung Choi,<sup>1,2</sup> Han-Sin Lee,<sup>1,2</sup> Gyuri Kim,<sup>1,2</sup> Geunsoo Kim,<sup>4</sup> Hyo Jun Park,<sup>4</sup> Pilhan Kim,<sup>3</sup> Sung Joo Kim,<sup>4</sup> and Jae Hyeon Kim<sup>1,2,5</sup>

*Diabetes* 2018;67:473–485 | <https://doi.org/10.2337/db17-0705>

**Highly angiogenic bone marrow mononuclear cell–derived spheroids (BM-spheroids), formed by selective proliferation of the CD31<sup>+</sup>CD14<sup>+</sup>CD34<sup>+</sup> monocyte subset via three-dimensional (3D) culture, have had robust angiogenic capacity in rodent syngeneic renal subcapsular islet transplantation. We wondered whether the efficacy of BM-spheroids could be demonstrated in clinically relevant intraportal islet transplantation models without increasing the risk of portal thrombosis. The thrombogenic potential of intraportally infused BM-spheroids was compared with that of mesenchymal stem cells (MSCs) and MSC-derived spheroids (MSC-spheroids). The angiogenic efficacy and persistence in portal sinusoids of BM-spheroids were examined in rodent syngeneic and primate allogeneic intraportal islet transplantation models. In contrast to MSCs and MSC-spheroids, intraportal infusion of BM-spheroids did not evoke portal thrombosis. BM-spheroids had robust angiogenic capacity in both the rodent and primate intraportal islet transplantation models and improved post-transplant glycemic outcomes. MRI and intravital microscopy findings revealed the persistence of intraportally infused BM-spheroids in portal sinusoids. Intraportal cotransplantation of allogeneic islets with autologous BM-spheroids in nonhuman primates further confirmed the clinical feasibility of this approach. In conclusion, cotransplantation of BM-spheroids enhances intraportal islet transplantation outcome without portal thrombosis**

**in mice and nonhuman primates. Generating BM-spheroids by 3D culture prevented the rapid migration and disappearance of intraportally infused therapeutic cells.**

Despite the encouraging results of the first multicenter phase 3 clinical trial in patients with type 1 diabetes complicated by severe hypoglycemia (1), the long-term metabolic outcome of clinical allogeneic islet transplantation is still not curative, even with potent immunosuppression (1–3). Although impaired revascularization of islet grafts in the portal sinusoid has long been considered one of the most important factors in the destruction of islet grafts in the early posttransplant period (4,5), no definite solution is clinically available. In this context, cotransplantation of bone marrow–derived mononuclear cells (BM-MNCs) and early or late endothelial progenitor cells with islets has been attempted and has shown promising results in small animal models (6–9), although the scarcity of the therapeutic cell population has been an obstacle to this approach. Recently, we tested a strategy to expand an autologous therapeutic cell population that possesses higher angiogenic or paracrine activities (10,11), namely, cotransplantation of islets with spheroids formed by selective *ex vivo* proliferation of the highly angiogenic CD31<sup>+</sup>CD14<sup>+</sup>CD34<sup>+</sup> monocyte subset via a three-dimensional (3D) culture technique that uses

<sup>1</sup>Division of Endocrinology and Metabolism, Department of Medicine, Samsung Medical Center, Sungkyunkwan University School of Medicine, Seoul, Republic of Korea

<sup>2</sup>Stem Cell and Regenerative Medicine Institute, Samsung Medical Center, Seoul, Republic of Korea

<sup>3</sup>Graduate School of Nanoscience and Technology, Korea Advanced Institute of Science and Technology, Daejeon, Republic of Korea

<sup>4</sup>Department of Surgery, Samsung Medical Center, Sungkyunkwan University School of Medicine, Seoul, Republic of Korea

<sup>5</sup>Department of Health Sciences and Technology, Samsung Advanced Institute for Health Sciences and Technology, Seoul, Republic of Korea

Corresponding author: Sung Joo Kim, [kmhyj111@gmail.com](mailto:kmhyj111@gmail.com), or Jae Hyeon Kim, [jaehyeon@skku.edu](mailto:jaehyeon@skku.edu).

Received 18 June 2017 and accepted 24 December 2017.

This article contains Supplementary Data online at <http://diabetes.diabetesjournals.org/lookup/suppl/doi:10.2337/db17-0705/-/DC1>.

B.J.O., S.-M.J., and Y.H. are the primary authors and contributed equally to this work. S.J.K. and J.H.K. are the senior authors and contributed equally to this work.

© 2018 by the American Diabetes Association. Readers may use this article as long as the work is properly cited, the use is educational and not for profit, and the work is not altered. More information is available at <http://www.diabetesjournals.org/content/license>.

a high cell density and nonattachable culture system (12). In our previous study, highly angiogenic bone marrow-derived spheroids (BM-spheroids) not only had robust angiogenic capacities, and actively participated in vessel formation *in vivo*, but also improved the survival and function of islet grafts in a mouse syngeneic marginal mass renal subcapsular islet transplantation model (12).

However, clinical application of this approach should be preceded by proof of its efficacy and safety in a clinically relevant intraportal islet transplantation model, in which loss of up to 60% of islets occurs in the first 2–3 days after transplantation, primarily because of the nonspecific inflammatory and thrombotic reaction called the instant blood-mediated inflammatory reaction (IBMIR) (13–15). The colocalization of islets with other therapeutic cells in portal sinusoids is another issue for the clinical application of this approach to intraportal islet transplantation because cotransplanted therapeutic cells could circulate throughout the whole body after intraportal injection, whereas islets are entrapped in the portal sinusoids. For reproduction of the benefits of their possible paracrine effects and direct incorporation into vessel formation in the renal subcapsular islet transplantation model in which islets and BM-spheroids are physically colocalized, the colocalization of BM-spheroids and islets in portal sinusoids should be secured in large-animal intraportal islet transplantation models. In addition, the safety of the therapeutic cells cotransplanted with islets should be documented in an intraportal islet transplantation model, with attention to previous studies that have reported that mesenchymal stem cells (MSCs) might not be compatible with human blood and might trigger IBMIR, depending on the cell dose and passage number (16). Thus, compatibility of BM-spheroids with recipient blood in the portal sinusoid should be confirmed before any human trial of this approach.

In this study, we wondered whether the robust angiogenic efficacy of BM-spheroids could be demonstrated in rodent and nonhuman primate (NHP) intraportal islet transplantation models without increasing the risk of portal thrombosis.

## RESEARCH DESIGN AND METHODS

### Animals

C57BL/6J or green fluorescent protein-transgenic (GFP-Tg) mice from the C57BL/6J background were obtained from The Jackson Laboratory (Bar Harbor, ME). Male GFP-Tg and wild-type C57BL/6J mice aged 10–12 weeks were used as donors and recipients, depending on the experiment. Diabetes was induced with streptozotocin (STZ) (Sigma-Aldrich, St. Louis, MO), administered intraperitoneally at 180 mg/kg in a citrate buffer solution (Sigma-Aldrich). Blood glucose concentration was measured with Accu-Chek glucose monitors (Roche, Mannheim, Germany) using blood from tail pinpricks. Diabetic mice with nonfasting blood glucose level  $\geq 400$  mg/dL for more than two consecutive days were used as recipients for islet grafts.

Cynomolgus monkeys (*Macaca fascicularis*) were 4–5 years of age and weighed 3–4 kg (Orient Bio Co. Ltd, Seongnam, Korea). Diabetes was induced with subtotal pancreatectomy followed by intravenous administration of 60–80 mg/kg STZ as previously described (17) (Supplementary Data). After induction of diabetes, all four NHPs satisfied all three of the following criteria (18): 1) sustained hyperglycemia (blood glucose level  $>250$  mg/dL), 2) fasting NHP C-peptide level consistently  $<1.0$  ng/mL or less than one-third of the pre-induction level, and 3) absence of stimulated C-peptide response with intravenous glucose tolerance test (IVGTT).

Mice experiments were approved by the institutional animal care and use committees (IACUCs) of Samsung Medical Center and the Korea Advanced Institute of Science and Technology. Monkey experiments were approved by the IACUCs of Samsung Medical Center and Orient Bio Laboratories.

### Spheroid Culture From BM-MNCs of Mice and NHPs

We performed 3D culture of mice and NHP BM-MNCs as previously described (12) (Supplementary Data). The experimental scheme for the intraportal cotransplantation of allogeneic islets and autologous BM-spheroids in the NHP model is shown in Supplementary Fig. 1A. Autologous BM-MNCs derived from the NHP recipients were counted and stored in liquid nitrogen until the diabetic NHP recipients received allogeneic NHP islet transplants. Frozen BM-MNCs were thawed and cultured for formation of spheroids 4–5 days before islet transplantation. The average size of the spheroids was  $108 \pm 4.3$   $\mu\text{m}$  (Supplementary Fig. 1B and C), and the average number of single cells per spheroid was  $2,063 \pm 831$  cells. The viability of the thawed BM-MNCs from three NHP recipients was  $\sim 90\%$ .

### Tracking of Intraportally Infused BM-Spheroids in Mice and NHPs

We tracked BM-spheroids labeled with ferucarbotran (Resovist; Bayer Schering Pharma AG, Berlin, Germany), a superparamagnetic iron oxide (SPIO), by MRI in the mouse and NHP models. GFP BM-spheroids derived from GFP-Tg mice were tracked by *ex vivo* bioluminescent imaging. To confirm the presence of the intraportally transplanted single cells dissociated from the BM-spheroids and intact BM-spheroids in the liver during the early posttransplant period, we used intravital microscopy (IVM) using a custom-built video-rate confocal microscopy platform as previously described (19, 20). Detailed methods of SPIO labeling and MRI (21), *ex vivo* bioluminescent imaging, and IVM imaging are available in the Supplementary Data.

### Mouse Pancreatic-Derived MSCs

Mouse pancreatic-derived MSCs (mPMSCs) were isolated from male GFP-Tg and wild-type C57BL/6J mice aged 10–12 weeks. Pancreatic cells left at the bottom after islet isolation by density gradient separation were washed in PBS and cultured with  $\alpha$ -minimum essential medium supplemented with 10% FBS and 1% penicillin/streptomycin. Medium was changed after 24–48 h to remove nonadherent

cells. When cultures reached confluence, cells were trypsinized and subcultured. In the current study, we used mPMSCs at passage 3. The cell surface marker pattern of the mPMSCs was analyzed by flow cytometry. The expression levels of genes with thrombogenic and proinflammatory properties in MSCs, MSC-derived spheroids (MSC-spheroids), and BM-spheroids were compared by microarrays and Western blot analysis (Supplementary Data).

### Intraportal Cotransplantation of Islets and BM-Spheroids in Mice and NHPs

Mice and NHP islets were isolated using a modified Ricordi method (22,23). In the murine models, cotransplantation of islets and BM-spheroids or dissociated BM-spheroid-derived single cells (dissociated BM-spheroids) and analysis of posttransplant outcome were performed in a syngeneic marginal mass mouse intraportal islet transplantation model.

In the NHP model, allogeneic marginal mass (20,000 islet equivalents [IEQ]/kg) of NHP islets (control group,  $n = 2$ ) and a mixture of allogeneic marginal mass (20,000 IEQ/kg) of NHP islets and NHP recipient autologous BM-spheroids (BM-spheroid group,  $n = 2$ : 35,750 spheroids in the BM-spheroid-1 recipient and 45,000 spheroids in the BM-spheroid-2 recipient) were transplanted with an immunosuppressive regimen used in a previous clinical study (24). Detailed methods of islet isolation, assessment of islet graft function, and immunohistochemistry of islet grafts are described in the Supplementary Data.

### Statistics

Values are expressed as the mean  $\pm$  SEM. The two groups were evaluated using an unpaired  $t$  test, and multiple comparisons between data were analyzed with one-way ANOVA. Statistical analyses were conducted using GraphPad Prism 4 software (GraphPad Software, La Jolla, CA), and a  $P$  value  $< 0.05$  was considered statistically significant.

## RESULTS

### Evaluation of Thrombogenesis After Intraportal Injection of MSCs, MSC-Spheroids, and BM-Spheroids

We first examined whether intraportal infusion of monolayer-cultured single MSCs (MSC-monolayers) and MSC-spheroids with various cell numbers per infusion evoked intraportal thrombosis. When cell-surface antigen expression was analyzed by flow cytometry, MSCs were positive for CD44, CD90.2, and Sca-1 but negative for CD31, CD34, CD45, CD117, and Flk-1 (Supplementary Fig. 2A). After 3 days of hanging drop culture, MSC-spheroids derived from different numbers ( $1 \times 10^3$ ,  $2.5 \times 10^3$ ,  $5 \times 10^3$ , and  $1 \times 10^4$ ) of MSCs had diameters that varied according to the number of source MSCs ( $116 \pm 11.03$   $\mu\text{m}$ ,  $170 \pm 13.73$   $\mu\text{m}$ ,  $210 \pm 12.61$   $\mu\text{m}$ , and  $272 \pm 21.19$   $\mu\text{m}$  in diameter, respectively) (Supplementary Fig. 2B and C). The real-time-PCR results indicated that the expression levels of angiogenic factors *Angpt1*, *Angpt2*, *Vegf*, *Fgf2*, *Igf1*, *Tgfb*, and *Plgf* are higher in MSC-spheroids than in MSC-monolayers (Supplementary Fig. 2D).

MSC-monolayers ( $1 \times 10^5$ ,  $2.5 \times 10^5$ , and  $5 \times 10^5$  cells),  $\sim 300$  MSC-spheroids containing  $3 \times 10^5$  cells ( $\sim 1 \times 10^3$  cells per spheroid [Sph  $1 \times 10^3$ ]), and  $\sim 100$  MSC-spheroids containing  $1 \times 10^6$  cells ( $\sim 1 \times 10^4$  cells per spheroid [Sph  $1 \times 10^4$ ]) were intraportally injected. After 24 h, we grossly observed the infarcted regions in the peripheral areas of livers that received MSC-monolayers and Sph  $1 \times 10^4$  (Fig. 1A). The livers that received Sph  $1 \times 10^3$  did not grossly show an infarction region. However, hematoxylin-eosin (H-E) staining revealed areas of necrosis accompanied by infiltration of neutrophils in all livers that received Sph  $1 \times 10^3$ , Sph  $1 \times 10^4$ , and MSC-monolayers (Fig. 1C). The infused GFP MSC-spheroids were tightly trapped in the CD31-stained blood vessels and observed in the proximity of the necrotic regions (Fig. 1D). Both H-E staining and GFP fluorescence revealed that the MSC-spheroids were responsible for the thrombosis (Fig. 1C and D). The GFP MSC-spheroids did not scatter throughout the whole liver (Supplementary Fig. 3). In contrast, the intraportally administered GFP MSC-monolayers, which caused most severe hepatic infarction, scattered throughout the whole liver (Supplementary Fig. 3).

We then examined whether thrombosis can be evoked by single cells dissociated from BM-spheroids (dissociated BM-spheroids) and intact BM-spheroids. Different numbers of dissociated BM-spheroids ( $5 \times 10^5$  and  $1 \times 10^6$  cells) or intact BM-spheroids (containing  $5 \times 10^5$ ,  $1 \times 10^6$ , and  $2 \times 10^6$  cells) were intraportally transplanted. Regardless of the infused cell number, no infarcted regions were grossly observed in the livers that received either dissociated BM-spheroids or intact BM-spheroids (Fig. 1B). Histologically, no infarcted regions were observed (Fig. 1C).

Next, we performed microarray analysis to investigate the differences in the genes involved in IBMIR between BM-spheroids and MSC-spheroids. Higher mRNA expression levels of genes with thrombogenic and proinflammatory properties (*TF*, *FBLN1*, *SERPINE1*, *CCL2*, *CCL8*, *CXCL12*, and *IL6*) were observed in MSC-spheroids than in BM-spheroids (Fig. 2A). Because *TF* (also known as coagulation factor III and *F3*) and *CCL2* are major coagulation and proinflammatory cytokines, we used Western blotting to examine difference in the protein levels of MSC-monolayers, MSC-spheroids, and BM-spheroids. The MSC-monolayers showed higher *TF* protein levels than the MSC-spheroids (up to  $5 \times 10^3$  cells/spheroid). The *TF* and *CCL2* protein levels were significantly lower in the BM-MNCs and BM-spheroids than in the MSC-monolayers and MSC-spheroids (Fig. 2C and D). Immunofluorescence also revealed that the infused MSC-monolayers and MSC-spheroids expressed *TF*, but the BM-spheroids did not (Fig. 2B).

### Cotransplantation of BM-Spheroids and Islets Improved Posttransplant Metabolic Outcomes of Mouse Syngeneic Intraportal Islet Transplantation

To examine whether cotransplantation of BM-spheroids and islets could enhance the outcomes from intraportal islet transplantation, we evaluated in vivo islet function using

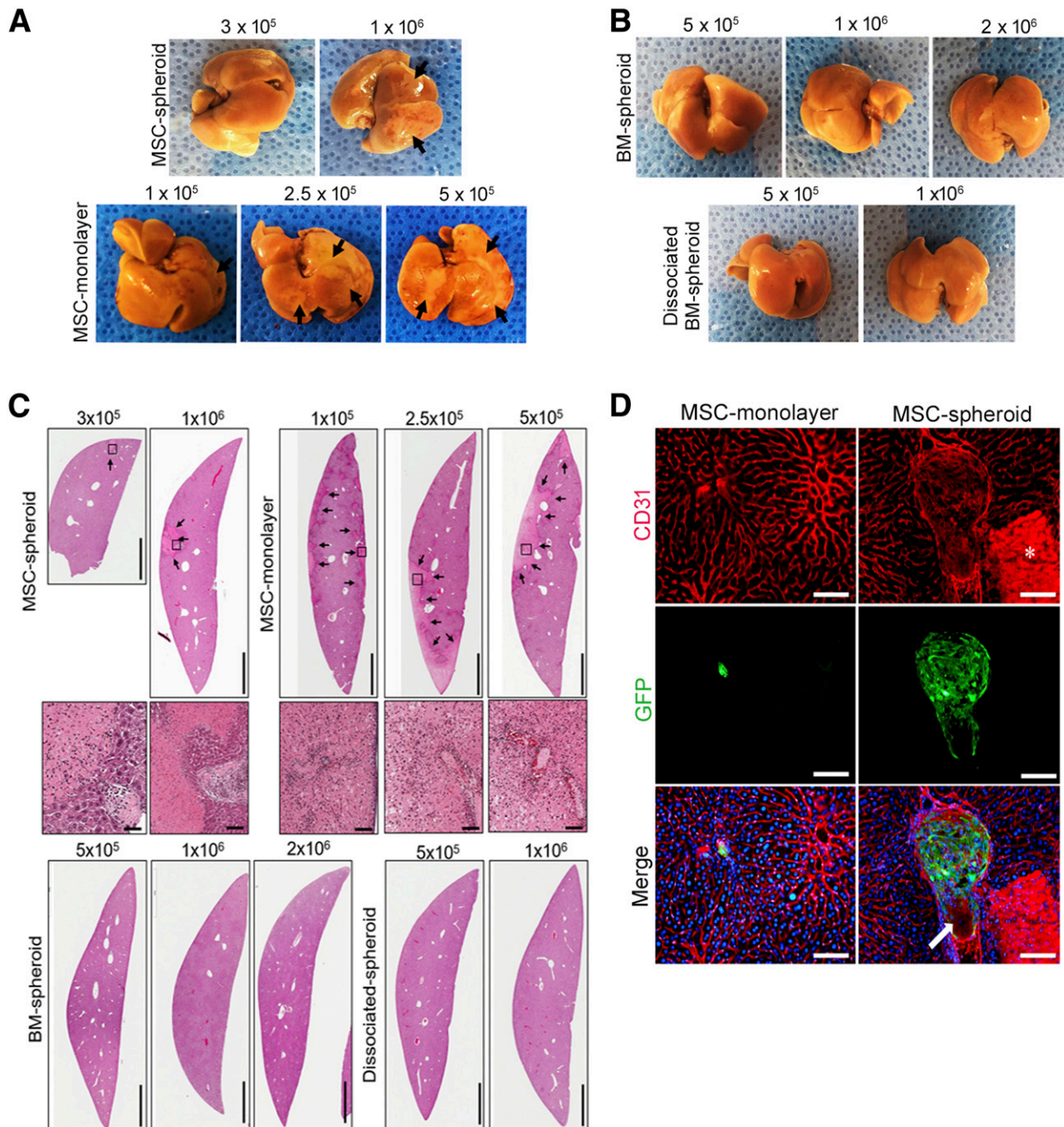


**Figure 1**—Histological assessment of liver tissue that received transplanted MSCs, MSC-spheroids, and BM-spheroids. **A**: Approximately 300 MSC-spheroids (containing  $3 \times 10^5$  cells [ $\sim 1 \times 10^3$  cells per spheroid]),  $\sim 100$  MSC-spheroids (containing  $1 \times 10^6$  cells [ $\sim 1 \times 10^4$  cells per spheroid]), and MSC-monolayers ( $1 \times 10^5$ ,  $2.5 \times 10^5$ , and  $5 \times 10^5$ ) were transplanted via the portal vein. After 24 h, each liver was extracted and observed for the presence of infarcted areas. Black arrows indicate the infarcted areas. **B**: Approximately 150 BM-spheroids (containing  $5 \times 10^5$  cells), 300 BM-spheroids (containing  $1 \times 10^6$  cells), 600 BM-spheroids (containing  $2 \times 10^6$  cells), and dissociated BM-spheroids ( $5 \times 10^5$  and  $1 \times 10^6$ ) were intraportally injected. Each liver was examined for the presence of infarcted areas. **C**: MSC-monolayers, MSC-spheroids, and BM-spheroids were transplanted via the portal vein. At DPT 1, liver tissues were prepared for H-E staining. Livers that received intraportally transplanted MSCs showed pathological changes, but those that received BM-spheroids did not. Arrows indicate infarction regions. Scale bars, 2 mm. Enlarged regions from the black square boxes indicate the infiltration of immune cells. Scale bars, 100  $\mu\text{m}$ . **D**: GFP MSC-monolayers and -spheroids were used to trace the behavior of MSC-monolayers and MSC-spheroids after intraportal injection. Liver tissues were stained with CD31 (red) for vessels and GFP (green) for MSCs. The asterisk indicates necrotic area, and the white arrow indicates blood clot formation. Scale bars, 100  $\mu\text{m}$ .

a syngeneic intraportal marginal mass (300 handpicked islets) islet transplantation model. As shown in Fig. 3A, diabetic mice received islets alone (islets alone group), islets

plus  $\sim 150$  BM-spheroids (containing  $5 \times 10^5$  cells [BM-spheroid group]), or islets plus single cells dissociated from the same number of BM-spheroids (dissociated

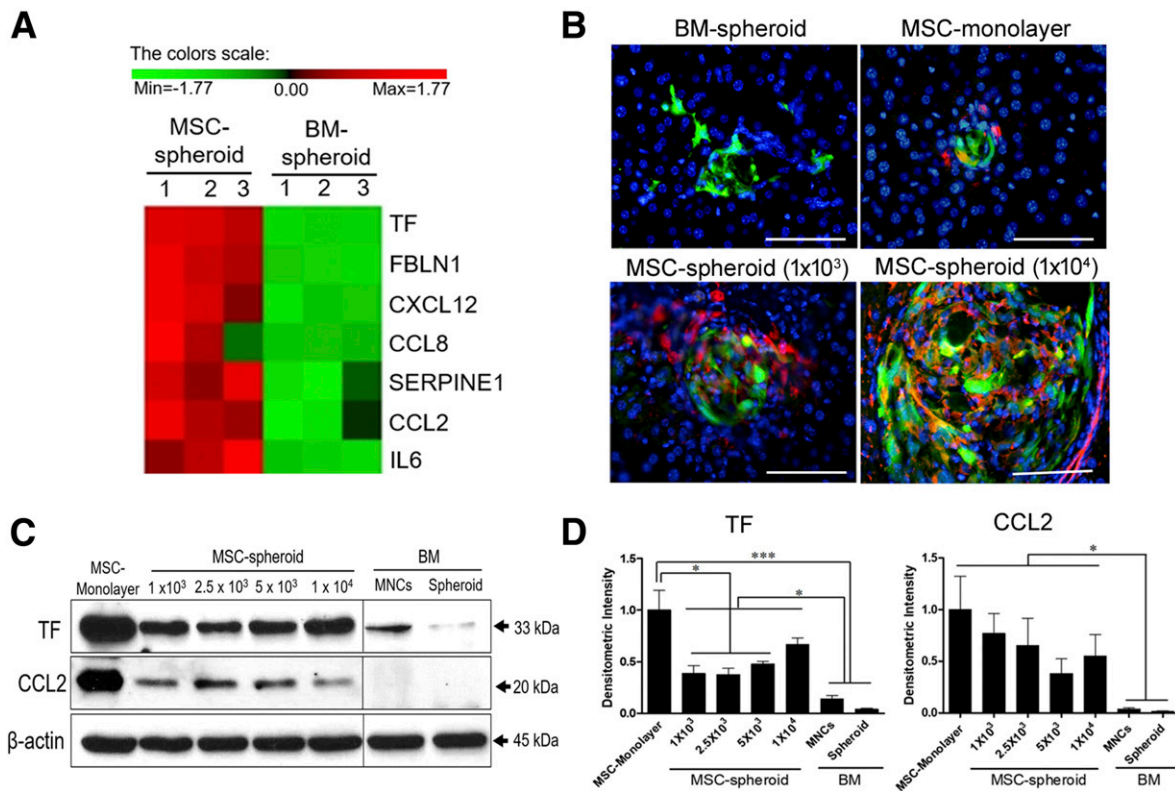


**Figure 2**—Coagulatory and inflammatory profiles of MSCs, MSC-spheroids, and BM-spheroids by microarray analysis and Western blot assay. **A:** Microarray analysis of the relative gene expression levels of BM-spheroids (test) and MSC-spheroids (control). Genes with  $P < 0.05$  and more than fourfold change in expression in three independent experiments were used to create the heat map, which was based on coagulatory and inflammatory gene expression profiles in BM-spheroids vs. MSC-spheroids. Red and green in the heat map indicate up- and downregulation in BM-spheroids compared with MSC-spheroids, respectively. **B:** Representative images of TF staining of intraportally injected GFP MSC-monolayers, MSC-spheroids, and BM-spheroids. Infused cells were stained with TF (red) and GFP (green). Scale bars, 100  $\mu\text{m}$ . **C** and **D:** Western blot analysis of TF and CCL2 protein levels was performed for MSC-monolayers, MSC-spheroids of different sizes ( $1 \times 10^3$  cells per spheroid,  $2.5 \times 10^3$  cells per spheroid,  $5 \times 10^3$  cells per spheroid, and  $1 \times 10^4$  cells per spheroid), BM-MNCs, and BM-spheroids. **C:** Representative immunoblotting. **D:** Quantitative analysis of band intensity. \* $P < 0.05$ ; \*\*\* $P < 0.001$ . The data are depicted as mean  $\pm$  SEM ( $n = 3$ ) values and normalized by  $\beta$ -actin. Max, maximum; Min, minimum.

BM-spheroid group) in the liver through the portal vein. Posttransplant blood glucose levels were lower in the BM-spheroid group than in the islets alone and dissociated BM-spheroid groups. The average blood glucose level of the BM-spheroid group was significantly lower than that of the islets alone ( $P < 0.01$ ) and dissociated BM-spheroid groups ( $P < 0.05$ ) at day posttransplantation (DPT) 28 (Fig. 3B–D). The diabetes reversal rate was also higher in the BM-spheroid group than in the islets alone and dissociated BM-spheroid groups (Fig. 3E). Intraportally glucose tolerance tests at DPT 28 revealed that glucose tolerance in the BM-spheroid group was significantly better than in the islets alone and dissociated BM-spheroid groups (Fig. 3F). The area under the curve for glucose was smaller in the BM-spheroid group than in the other groups (Fig. 3G). Serum insulin concentrations before and 30 min after glucose injection were also higher in the BM-spheroid group than in the other groups (Fig. 3H).

Next, we intraportally cotransplanted lower numbers of BM-spheroids ( $1 \times 10^5$  cells [lower number BM-spheroid group]) with islets and compared that outcome with outcomes

from intraportal islet transplantation with or without concurrent tail vein injection of higher numbers ( $0.5\text{--}1 \times 10^6$  cells) of single cells dissociated from BM-spheroids (tail vein dissociated BM-spheroid group) (Supplementary Fig. 4A). The posttransplant blood glucose level, diabetes reversal rate, and glucose tolerance were markedly improved in the lower number BM-spheroid group compared with those in the islets alone and tail vein dissociated BM-spheroid groups (Supplementary Fig. 4B–G).

#### Cotransplanting BM-Spheroids and Islets Improved Islet Composition and Enhanced Revascularization in Mouse Syngeneic Intraportal Islet Transplantation

Islet morphology and vessel density were assessed in graft-bearing livers at DPT 28. Islets were detected within the liver parenchyma and around the portal venules in all groups. Insulin staining of intraportally transplanted islets indicated more intact islet morphology in the BM-spheroid group than in the other groups (Fig. 4A). The fractional  $\beta$ -cell area, islet size, and islet number/total area of the

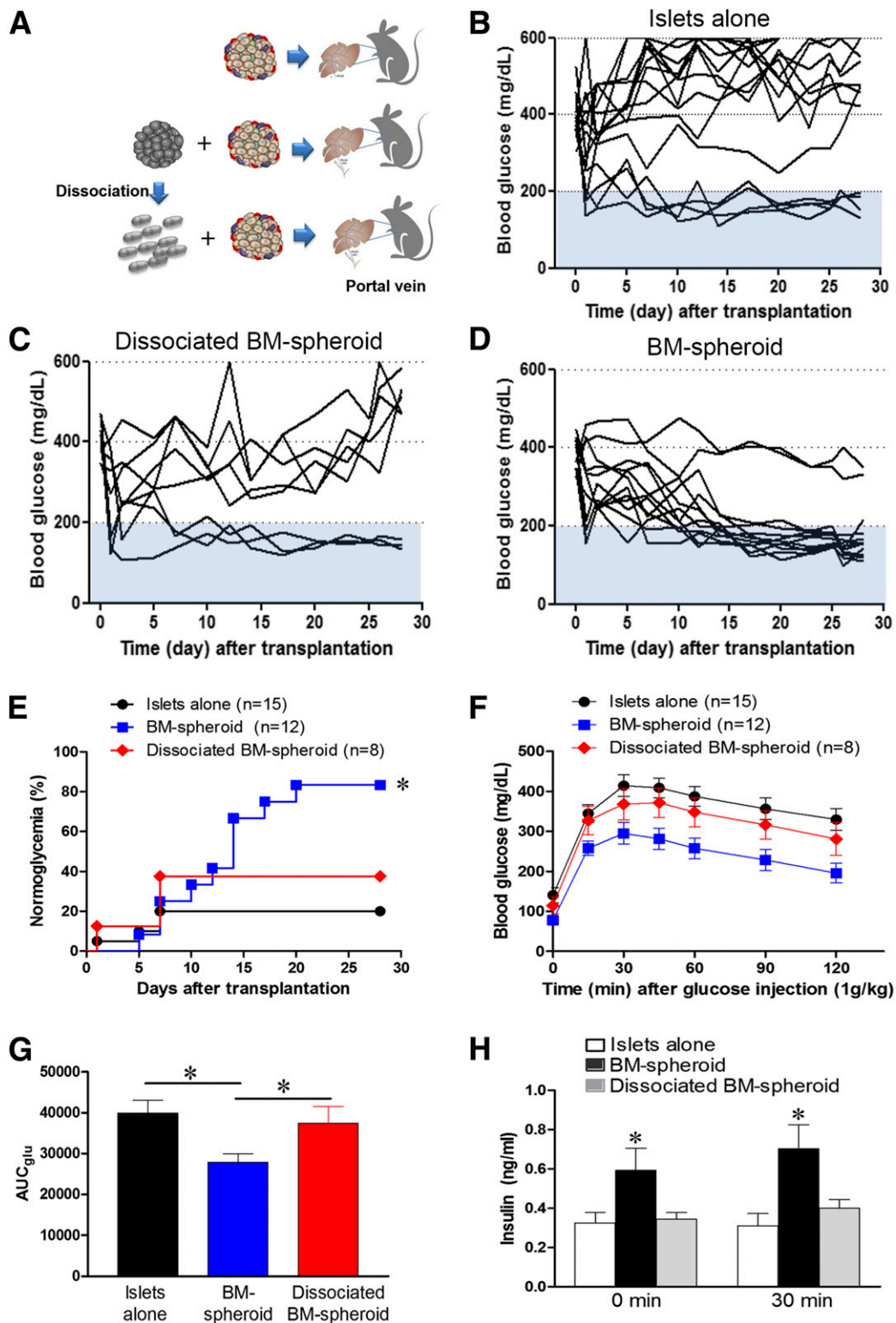


**Figure 3**—Reversal of diabetes after intraportal cotransplantation of BM-spheroids and islets. **A**: Experimental scheme of intraportal cotransplantation of islets and BM-spheroids. Experimental animals were divided into three groups: islets alone (300 handpicked islets), islets (300 islets) plus 150–200 BM-spheroids, and islets (300 islets) plus  $5 \times 10^5$  single cells dissociated from BM-spheroids. Islets and BM-spheroids were cotransplanted through the portal vein of mice with STZ-induced diabetes. **B–D**: Blood glucose concentration of mice intraportally transplanted with islets alone ( $n = 15$ ) (islets alone group) (B), islets plus BM-spheroids ( $n = 12$ ) (BM-spheroid group) (D), or islets plus single cells dissociated from BM-spheroids ( $n = 8$ ) (dissociated BM-spheroid group) (C) was measured up to DPT 28. The mean blood glucose level was  $399 \pm 52$  mg/dL in islets alone,  $375 \pm 69$  mg/dL in dissociated BM-spheroid, and  $184 \pm 23$  mg/dL in BM-spheroid at DPT 28. **E**: Cumulative diabetes reversal curve after islet transplantation. Normoglycemia was defined as  $<200$  mg/dL on consecutive days. \* $P < 0.05$  for log-rank test of islets alone (4/15) or dissociated BM-spheroid (3/8) vs. BM-spheroid (12/14). **F**: Glucose tolerance test at DPT 28. Blood glucose levels were measured

BM-spheroid group were significantly greater than those in the other groups (Fig. 4B–D). The relative distribution of the glucagon-positive cells did not differ between groups (Supplementary Fig. 5A). For identification of whether BM-spheroids remained within the recipient liver, BM-spheroids from GFP-Tg mice (GFP BM-spheroids) and dissociated single cells from GFP BM-spheroids (GFP dissociated BM-spheroids) were cotransplanted with islets via the portal vein. Transplanted GFP BM-spheroids were found throughout the recipient liver at DPT 14 and 28, whereas GFP dissociated BM-spheroids were rarely observed (Fig. 4E and Supplementary Fig. 5B). The vascular density of the insulin-positive area in the BM-spheroid group was significantly higher than that in the islets alone and dissociated BM-spheroid groups at DPT 14 and 28, even without incorporation of GFP BM-spheroids into the intraislet vasculatures (Fig. 4F–H).

When the islet grafts in the experiments depicted in Supplementary Fig. 4 were analyzed, the lower number BM-spheroid group showed higher fractional  $\beta$ -cell area, islet size, islet number/total area, and vascular density of insulin-positive area than the islets alone and tail vein dissociated BM-spheroid groups (Supplementary Fig. 6).

When the recipient pancreata in each experiment were analyzed, insulin-stained cells were rarely observed, and even if observed, the insulin-positive cells comprised only an extremely small fraction of pancreatic islets (Supplementary Fig. 7A).

#### Distribution of Dissociated or Intact BM-Spheroids in the Livers of Syngeneic Mouse Recipients After Intraportal Injection

After injecting GFP dissociated BM-spheroids or intact GFP BM-spheroids via the portal vein, we used bioluminescent imaging to trace the transplanted GFP cells in the spleen, lung, and liver at DPT 1. Most of the intact GFP BM-spheroids accumulated in the liver—not in the lung or spleen. However, GFP dissociated BM-spheroids showed lower fluorescence intensity in the liver than intact GFP BM-spheroids and high fluorescence intensity in the lung (Fig. 5A).

In parallel, we aimed to confirm the distribution of BM-spheroids in recipient livers using MRI of SPIOs. BM-MNCs were labeled with ferucarbotran for 24 h and then cultured for 4 days to form BM-spheroids. Ex vivo MRI of BM-spheroids labeled with ferucarbotran revealed visible hypointense spots representing the labeled BM-spheroids (Fig. 5B). The labeling agent did not compromise the viability or 3D formation of BM-spheroids during the culture period (data not shown). When we infused the ferucarbotran-labeled dissociated BM-spheroids or ferucarbotran-labeled intact BM-spheroids via the portal vein, the number of hypointense spots representing the labeled

cells in the BM-spheroid group was greater than that in the dissociated BM-spheroid group at DPT 1 and 8 (Fig. 5C).

To confirm the presence of the intraportally transplanted dissociated BM-spheroids and intact BM-spheroids in the liver during the early posttransplant period, we obtained IVM images. The number of fluorescent spots representing intact GFP BM-spheroids was greater than the number representing GFP dissociated BM-spheroids at DPT 0, 1, and 7. Variable sizes of GFP BM-spheroids were detectable at DPT 0, and their shapes were rarely spherical (Fig. 5D). GFP dissociated BM-spheroids rapidly disappeared over time, so that no fluorescent spots representing GFP dissociated BM-spheroids were observed at DPT 7 (Fig. 5D). Collectively, these results indicate that the BM-spheroids are trapped within the liver, whereas dissociated BM-spheroids drain into the systemic circulation.

#### Cotransplantation of BM-Spheroids and Islets in NHP Allogeneic Intraportal Marginal Mass Islet Transplantation

To confirm the localization of NHP autologous BM-spheroids within the recipient liver, we first autologously transplanted NHP BM-spheroids labeled with an SPIO (ferucarbotran). At DPT 2, an MRI of the recipient liver revealed hypointense spots representing the labeled BM-spheroids (Fig. 6A). At DPT 17, the NHP was sacrificed, and ex vivo MRI of the liver and iron staining were performed. In this analysis, the hypointense spots were confirmed to represent Prussian blue-stained BM-spheroids (Fig. 6B). In addition, we found no evidence of thrombosis in the portal veins or venules (data not shown).

We then transplanted an allogeneic marginal mass (20,000 IEQ per recipient's body weight in kilograms) of NHP islets with (BM-spheroid group) or without (control group) the NHP recipient's autologous BM-spheroids into NHP recipients with STZ-induced diabetes ( $n = 2$  per each group).

In the immunohistochemistry analysis of the recipient livers in the control group, the majority of the graft sites were infiltrated with many T cells and macrophages, and only a few islets showed successful engraftment (Fig. 6C), resulting in negligible fractional  $\beta$ -cell areas (Fig. 6D). In contrast, the immunohistochemistry analysis of the recipient livers in the BM-spheroid group revealed intact islet grafts with minimal infiltration of T cells and macrophages. CD31-positive vessels were observed in the periphery of the islets or within insulin-positive endocrine areas in the BM-spheroid group but not in the control group (Fig. 6C). The insulin-positive area in the BM-spheroid group was larger than that in the control group (Fig. 6D). There was no evidence of portal vein thrombosis or infarction of the liver in either group of recipients (data not shown).

at 0, 15, 30, 45, 60, 90, and 120 min after glucose (1 g/kg) injection. G: Area under the curve ( $AUC_{G_{i(t)}}$ ) for intraperitoneal glucose tolerance test. \* $P < 0.05$ . H: Fasting serum insulin levels at 0 and 30 min after glucose loading. \* $P < 0.05$ , one-way ANOVA followed by Tukey multiple comparisons test.

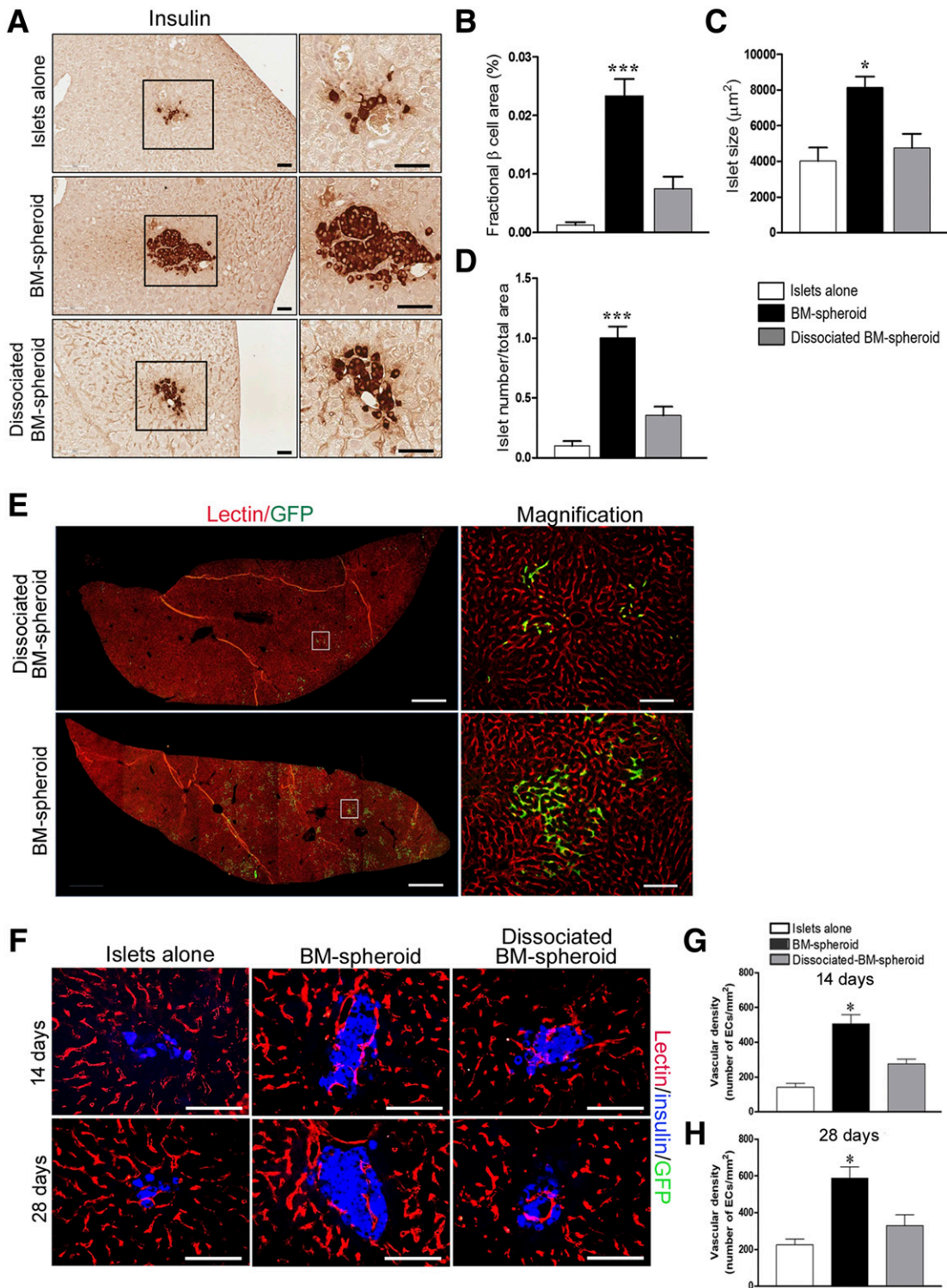


**Figure 4**—Assessment of morphology and revascularization for graft-bearing liver cotransplanted with BM-spheroids. **A**: At DPT 28, the graft-bearing liver tissues were stained for insulin. Representative images of islets transplanted via the portal vein are shown. Regions denoted by a black line indicate magnified images (right panel). Scale bars, 50  $\mu\text{m}$ . **B–D**: Evaluation of fractional  $\beta$ -cell area (**B**), islet size (**C**), and islet number/total area (**D**) for the grafted tissues of each group. \* $P < 0.05$ ; \*\*\* $P < 0.001$ . **E**: For tracing of the transplanted BM-spheroids and functional vessels, GFP BM-spheroids derived from GFP-Tg mice were cotransplanted with islets, and rhodamine-labeled BS1 lectin was intracardially injected. Liver tissues were stained with GFP antibody to determine how many GFP cells were present at DPT 14. Regions denoted by a white line indicate magnified images (right panel). Scale bars of left panel, 1 mm, and scale bars of right panel, 100  $\mu\text{m}$ . **F**: At DPT 14 and 28, representative images indicate vessel formation at the graft site. Vessels, islets, and GFP BM-spheroids were stained for lectin (red), insulin (blue), and GFP (green). Scale bars, 100  $\mu\text{m}$ . **G** and **H**: Quantification of the vessel density of each group at DPT 14 (**G**) and DPT 28 (**H**). \* $P < 0.05$ , one-way ANOVA followed by Tukey multiple comparisons test. ECs, endothelial cells.

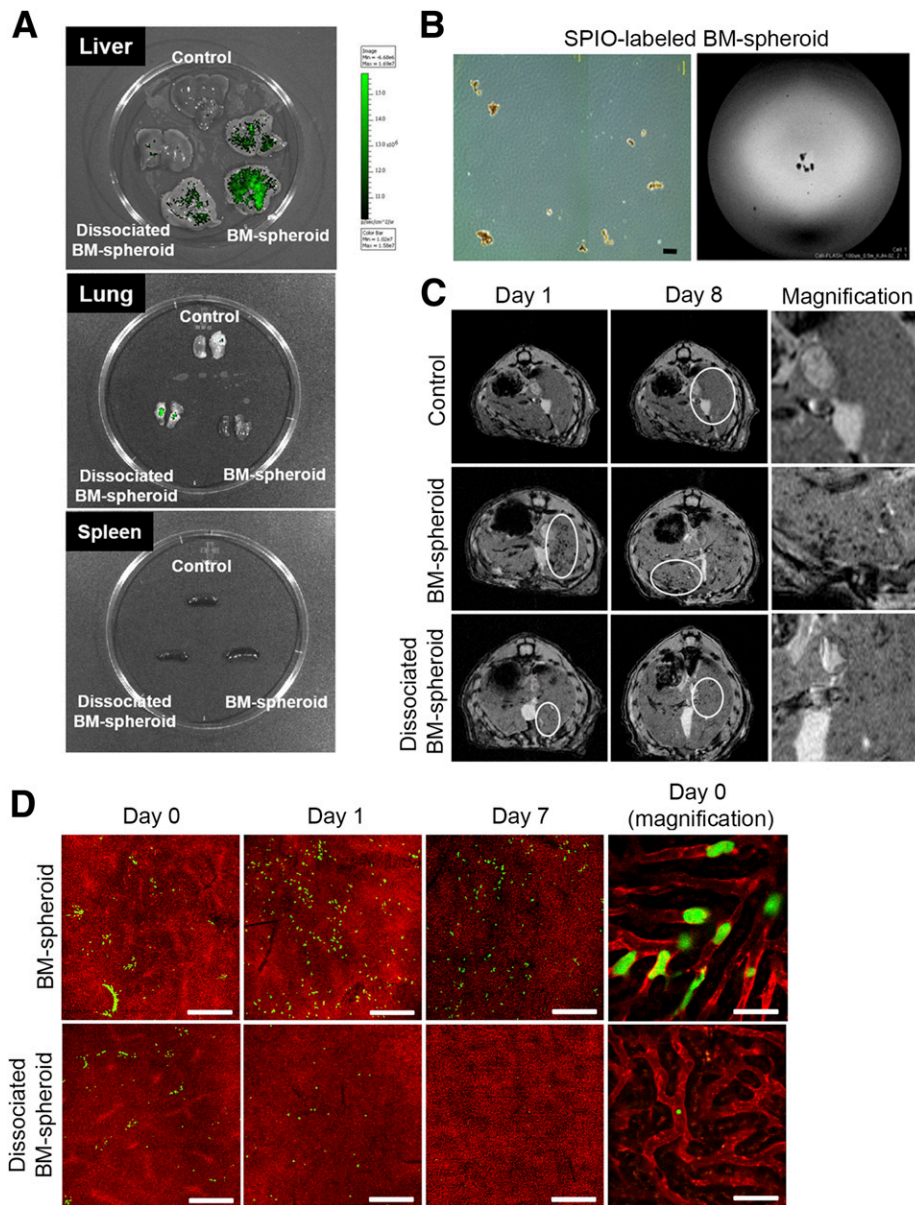


**Figure 5**—Tracing of transplanted BM-spheroids. **A:** Bioluminescent imaging. GFP BM-spheroids and GFP dissociated BM-spheroids were intraportally transplanted. Mice of each group were injected with the same number of GFP cells ( $1 \times 10^6$  cells). Liver, spleen, and lung were imaged at DPT 1. Control is the liver without transplanted GFP BM-spheroids. The single bar indicates relative photon light intensity. **B:** Cell ex vivo MRI. The cell imaging of BM-spheroids labeled with ferucarbotran was performed by MRI. The left panel is a BM-spheroid image obtained by optical microscopy, and the right panel is visible hypointense spots representing ferucarbotran-labeled BM-spheroids. Scale bar, 100  $\mu\text{m}$ . **C:** Liver MRI images of ferucarbotran-labeled BM-spheroids and dissociated BM-spheroids transplanted via the portal vein. MRI images were obtained at DPT 1 and 8. Control is liver MRI images without transplanted BM-spheroids. White elliptical regions are distinctly visible hypointense spots representing ferucarbotran-labeled BM-spheroids and dissociated BM-spheroids. Enlarged regions from white elliptical regions of the middle panel are shown in the right panel. **D:** IVM for monitoring transplanted BM-spheroids. IVM was performed using the same method described in **A** and obtained at DPT 0, 1, and 7. Mice were injected with Alexa Fluor 647-conjugated CD31 antibody (vessel staining shown in red) via tail vein before GFP BM-spheroid transplantation. Scale bars, 500  $\mu\text{m}$ . Right panel shows high-magnification views of vessel-entrapped spheroids (upper) and GFP single cells (lower). Scale bar, 25  $\mu\text{m}$ . Max, maximum; Min, minimum.

The two recipients in the control group continued to receive exogenous insulin, with the doses reduced from those before islet transplantation, whereas the post-transplant blood glucose levels were maintained within the target range (random glucose  $<200$  mg/dL) without administration of exogenous insulin in the two recipients

in the BM-spheroid group (Fig. 7). In the recipient pancreata of control and BM-spheroid groups, insulin-stained cells were rarely observed, and even if observed, the insulin-positive cells comprised only an extremely small fraction of pancreatic islets (Supplementary Fig. 7B).

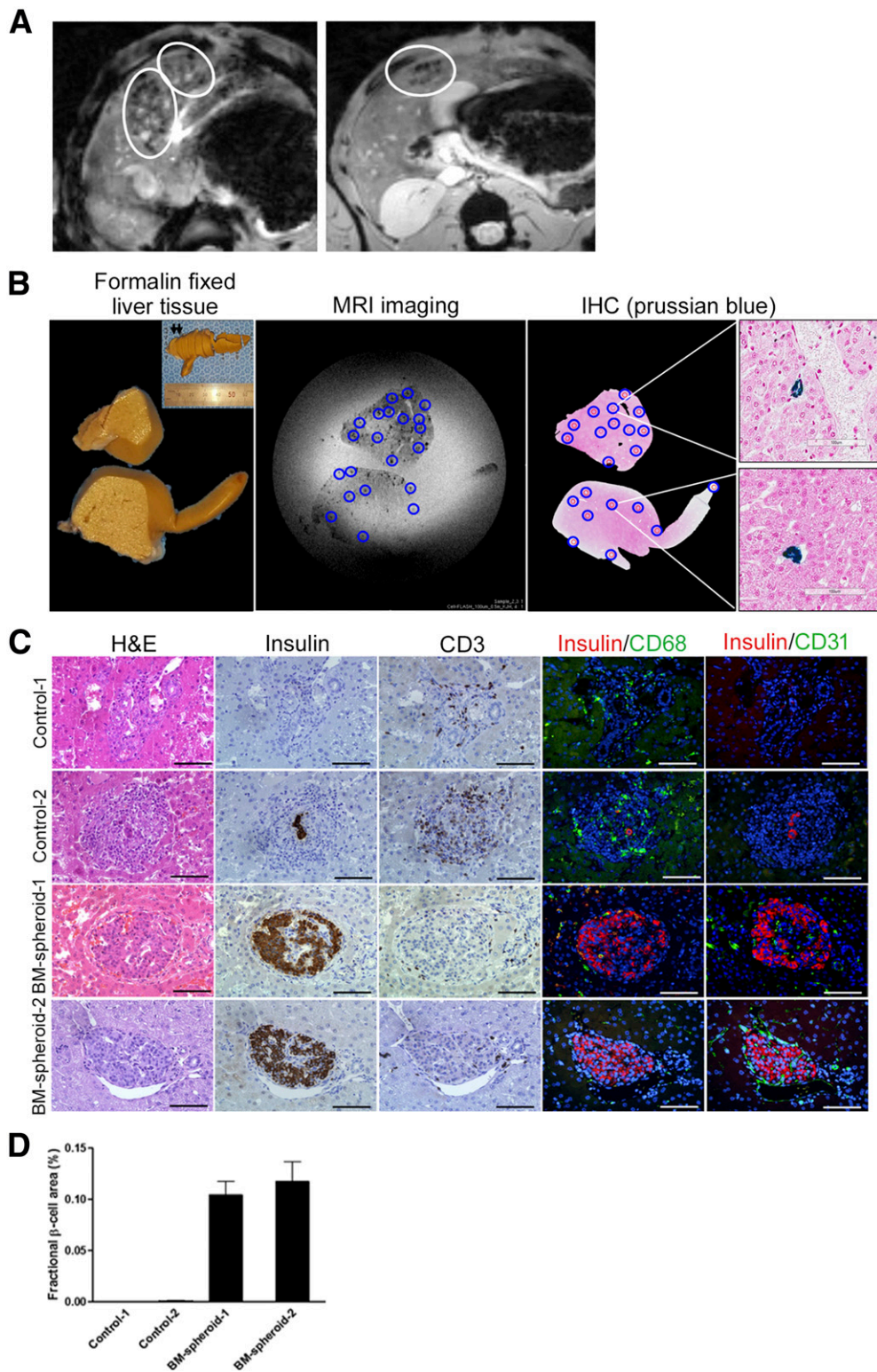


**Figure 6**—MRI imaging of NHP BM-spheroids and immunohistochemical (IHC) staining of graft-bearing livers. *A*: In the NHP model, NHP BM-MNCs were labeled with ferucarbotran for 24 h and then cultured for 3 days to form BM-spheroids. Ferucarbotran-labeled NHP BM-spheroids were transplanted via the portal vein and observed by MRI at DPT 2. White elliptical regions indicate visible hypointense spots from ferucarbotran-labeled NHP BM-spheroids. *B*: Concurrent tissue ex vivo MRI and histological analysis. A monkey was sacrificed at DPT 17, and liver tissues were obtained for tissue ex vivo MRI and iron staining. Left panel: liver tissues sliced from the caudate lobe of the liver (arrows of top-right corner inset). Middle panel: ex vivo MRI imaging of the liver slices shown in the left panel. Right panel: Prussian blue staining for iron in the same tissue section; blue circles indicate the correspondence of hypointense spots and Prussian blue staining, and the upper and lower panels are magnified views of iron staining (blue). Scale bars, 100  $\mu$ m. *C*: Livers were obtained from control-1, control-2, BM-spheroid-1, and BM-spheroid-2 at DPT 90, 90, 36, and 191, respectively. Live tissues were stained with anti-insulin, CD3, CD68, and CD31 antibodies to reveal

## DISCUSSION

The 3D culture models allow various cells to behave more like *in vivo* cells, providing enhanced therapeutic efficacy (25) and local persistence of therapeutic cells (26). In the current study, the robust angiogenic efficacy of the BM-spheroids in our previous study (12) was reproduced in more clinically relevant intraportal islet transplantation models, and the BM-spheroids did not evoke portal thrombosis even when the infused cell number far exceeded the number of MSCs that caused liver infarction after intraportal injection in parallel experiments.

In this study, generating BM-spheroids by 3D culture prevented the rapid migration and disappearance of intraportally infused therapeutic cells. This was in contrast to the behavior of dissociated BM-spheroids in this study and MSC-monolayers in a previous study (27), which rapidly drained to the systemic circulation and became trapped in the lung after administration. The benefit of cotransplanted BM-spheroids likely depends on their colocalization with islets in portal sinusoids because dissociated BM-spheroids did not retain the benefit of islet engraftment, even with greater cell numbers than used for the intact BM-spheroids, regardless of the administration route. Given the extraislet location of GFP BM-spheroids suggesting paracrine mechanism and the rapid time course of revascularization and glycemic benefit, the main mechanism for the angiogenic efficacy of BM-spheroids is likely to be a paracrine effect rather than a direct incorporation or a systemic effect. In addition, the reduced infiltration of T cells in the islet grafts (Fig. 6C) could be another explanation for the angiogenic efficacy of BM-spheroids because the effector T-cell cytokine interferon- $\gamma$  has been shown to be antiangiogenic in tumor (28) and lung ischemia models (29).

The thrombogenicity of MSC-spheroids in portal sinusoids is another novel finding of this study. Although little attention has been given to it, MSCs provoke IBMIR (16), and that could contribute to their lack of persistence in target tissue. Even though we used short-term expanded MSCs (three passages) with less procoagulant activity than MSCs with higher passage numbers, the infused MSC-monolayers scattered throughout the whole liver and caused extensive portal thrombogenesis regardless of infused cell number. Interestingly, both thrombogenicity and the increase in the level of *TF* expression were attenuated in MSC-spheroids compared with MSC-monolayers. The GFP MSC-spheroids did not scatter throughout the whole liver, with much less portal thrombosis than that of MSC-monolayers (Supplementary Fig. 3). In contrast to the MSC-monolayers and MSC-spheroids, the nonthrombogenicity of BM-spheroids was histologically proven in this study and was further supported by low expression levels of *TF* and *CCL2*.

The results of our pilot NHP study, which used a readily available immunosuppressive regimen, supported the clinical feasibility of cotransplantation of allogeneic islets and autologous BM-spheroids. We also demonstrated the localization of BM-spheroids in the liver of NHP recipients using a 4.7T preclinical MRI of SPIO-labeled BM-spheroids. For clinical application, this strategy has several practical benefits. First, we derived the autologous BM-spheroids from precollected bone marrow from the recipient monkey. We froze the bone marrow and thawed it immediately before islet isolation. This is compatible with actual clinical settings for allogeneic islet transplantation, in which isolated islets are typically cultured for up to 3 days (1). Second, the procedure does not require surface modification of transplanted islets, which usually causes loss of therapeutic islet mass due to structural destruction of isolated islets. This is in contrast to other approaches, such as encapsulation of islets (30), islet surface camouflage (31,32), and coating the islet surface with endothelial cells (33) or endothelial progenitor cells (7). Third, our histological analysis of the recipient liver revealed small, elliptical BM-spheroids in more peripheral areas of the liver than the areas containing islet grafts. This morphological transformation of BM-spheroids might have contributed to the lack of hepatic infarction after infusion of the BM-spheroids into the portal sinusoids. In this context, it is also reassuring that cotransplantation of islets with a lower number of BM-spheroids (approximately one-third that of the cotransplanted islet cells) still produced the benefit.

This study had several limitations that should be discussed. Although portal thrombosis was evoked by MSCs in our experiments, the results of this study should not be interpreted as denial of the clinical feasibility of MSC-islet cotransplantation because various studies on the optimization of 3D culture methods and biomaterial-based modification are ongoing (34,35). In addition, we failed to prove the difference in C-peptide response after intravenous glucose challenge between the groups in NHP experiments. Although posttransplant body weight was stable in all the NHP recipients and all the recipient pancreata had minimal fraction of insulin-stained cells in this study, the findings of our NHP pilot study should be confirmed by further study with better control of possible model-induced confounding factors such as insufficient insulin secretion due to the marginal mass of islet graft, as well as malabsorptive caloric reduction due to the immunosuppressant-induced gastrointestinal toxicity (36,37).

In conclusion, cotransplantation of angiogenic monocyte subset spheroids derived from BM-MNCs enhances intraportal islet transplantation outcomes without portal thrombosis in mice and NHPs. In addition to their robust angiogenic capacity *in vivo*, 3D culture-formed BM-spheroids

---

NHP  $\beta$ -cells, T cells, macrophages, and vessels, respectively. Islets from normoglycemic BM-spheroid-1 and BM-spheroid-2 show intact morphology and are devoid of immune cell infiltration, whereas the control group of islets alone showed no insulin-positive  $\beta$ -cells or CD31-stained vessel cells and was occupied by immune cells. Scale bars, 100  $\mu$ m. *D*: Quantification of the  $\beta$ -cell areas (%) in control-1, control-2, BM-spheroid-1, and BM-spheroid-2. H&E, hematoxylin-eosin.

---

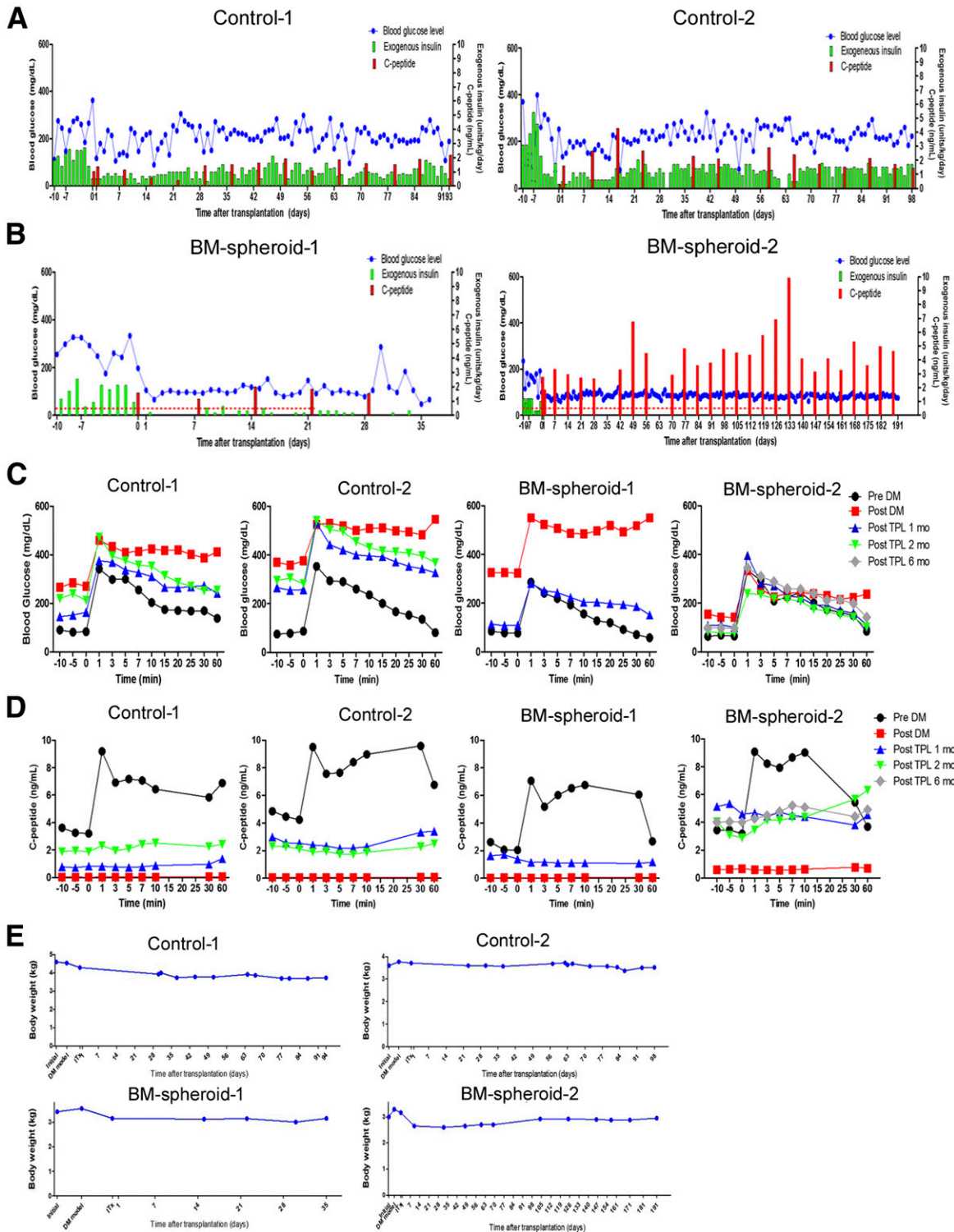


**Figure 7**—Blood glucose control by cotransplantation of islets and NHP BM-spheroids. *A* and *B*: Fasting blood glucose level and monkey C-peptide were measured in two monkeys that received intraportal transplants of allogeneic monkey islets (20,000 IEQ/kg) (*A*) and two monkeys that received cotransplants of allogeneic monkey islets (20,000 IEQ/kg) (*B*) and autologous recipient BM-spheroids via the portal vein. The control-1 and control-2 monkeys were insulin dependent until the end of the experiment (at DPT 93 and 98, respectively), whereas the BM-spheroid-1 monkey was insulin independent for 36 days (before sacrifice) and the BM-spheroid-2 monkey continued to maintain normoglycemia without insulin injection until the end of the experiment (at DPT 191). Blue line, blood glucose levels; red bar, monkey C-peptide; green bar, exogenous insulin. *C*: IVGTT. An IVGTT was performed at the indicated time points and examined before and after diabetes (DM) and 1, 2, and 6 months (mo) posttransplantation (post TPL). *D*: C-peptide secretion in response to glucose load. Before induction of diabetes, monkey C-peptide was normally detected after glucose injection; after induction of diabetes, monkeys showed C-peptide levels <1.0 ng/mL. *E*: The body weight change after islet transplantation in each recipient.

provided additional benefits in terms of localized persistence in portal sinusoids.

**Funding.** This research was supported by grants from the Samsung Biomedical Research Institute (GL1B30811), the National Research Foundation of Korea (NRF-2015R1A2A2A01003509, NRF-2015R1A2A1A1A5053895), and the Korea Health Technology R&D Project through the Korea Health Industry Development Institute, funded by the Ministry of Health and Welfare (A084065 and H12C1853).

**Duality of Interest.** No potential conflicts of interest relevant to this article were reported.

**Author Contributions.** B.J.O., S.-M.J., S.J.K., and J.H.K. conceived the work, designed the experiments, and wrote the manuscript. B.J.O. and J.M.C. performed intraportal transplantation using MSCs, MSC-spheroids, and BM-spheroids. H.-S.L., Ge.K., and H.J.P. conducted NHP experiments. Y.H. and P.K. performed IVM images and ex vivo bioluminescent imaging. B.J.O. and J.M.C. assisted with the microarray analysis and tissue staining. B.J.O., S.-M.J., and Gy.K. acquired data and analyzed data. S.J.K. and J.H.K. are the guarantors of this work and, as such, had full access to all the data in the study and take responsibility for the integrity of the data and the accuracy of the data analysis.

## References

- Hering BJ, Clarke WR, Bridges ND, et al.; Clinical Islet Transplantation Consortium. Phase 3 trial of transplantation of human islets in type 1 diabetes complicated by severe hypoglycemia. *Diabetes Care* 2016;39:1230–1240
- Lablanche S, Borot S, Wojtuszczyzn A, et al.; GRAGIL Network. Five-year metabolic, functional, and safety results of patients with type 1 diabetes transplanted with allogenic islets within the Swiss-French GRAGIL network. *Diabetes Care* 2015;38:1714–1722
- Qi M, Kinzer K, Danielson KK, et al. Five-year follow-up of patients with type 1 diabetes transplanted with allogeneic islets: the UIC experience. *Acta Diabetol* 2014;51:833–843
- Brissova M, Fowler M, Wiebe P, et al. Intraislet endothelial cells contribute to revascularization of transplanted pancreatic islets. *Diabetes* 2004;53:1318–1325
- Brissova M, Powers AC. Revascularization of transplanted islets: can it be improved? *Diabetes* 2008;57:2269–2271
- Kang S, Park HS, Jo A, et al. Endothelial progenitor cell cotransplantation enhances islet engraftment by rapid revascularization. *Diabetes* 2012;61:866–876
- Kim JH, Oh BJ, Lee HN, Park HS, Park SG, Park KS. Endothelial colony-forming cell coating of pig islets prevents xenogeneic instant blood-mediated inflammatory reaction. *Cell Transplant* 2011;20:1805–1815
- Oh BJ, Oh SH, Jin SM, et al. Co-transplantation of bone marrow-derived endothelial progenitor cells improves revascularization and organization in islet grafts. *Am J Transplant* 2013;13:1429–1440
- Sakata N, Chan NK, Chrisler J, Obenaus A, Hathout E. Bone marrow cell cotransplantation with islets improves their vascularization and function. *Transplantation* 2010;89:686–693
- Hur J, Choi JI, Yun JY, et al. Highly angiogenic CXCR4(+)/CD31(+) monocyte subset derived from 3D culture of human peripheral blood. *Biomaterials* 2013;34:1929–1941
- Hur J, Park J, Lee SE, et al. Human peripheral blood-borne hematopoietic stem cell niche for hematopoietic stem cell expansion. *Cell Res* 2011;21:987–990
- Oh BJ, Jin SM, Choi JM, et al. Improved revascularization of islet grafts using an angiogenic monocyte subpopulation derived from spheroid culture of bone marrow mononuclear cells. *Am J Transplant* 2015;15:1543–1554
- Davalli AM, Scaglia L, Zangen DH, Hollister J, Bonner-Weir S, Weir GC. Vulnerability of islets in the immediate posttransplantation period. Dynamic changes in structure and function. *Diabetes* 1996;45:1161–1167
- Bennet W, Sundberg B, Groth CG, et al. Incompatibility between human blood and isolated islets of Langerhans: a finding with implications for clinical intraportal islet transplantation? *Diabetes* 1999;48:1907–1914
- Moberg L, Johansson H, Lukinius A, et al. Production of tissue factor by pancreatic islet cells as a trigger of detrimental thrombotic reactions in clinical islet transplantation. *Lancet* 2002;360:2039–2045
- Moll G, Rasmusson-Duprez I, von Bahr L, et al. Are therapeutic human mesenchymal stromal cells compatible with human blood? *Stem Cells* 2012;30:1565–1574
- Park H, Park JB, Kim JH, et al. Simultaneous subtotal pancreatectomy and streptozotocin injection for diabetes modeling in cynomolgus monkeys. *Transplant Proc* 2017;49:1142–1149
- Cooper DK, Casu A. The International Xenotransplantation Association consensus statement on conditions for undertaking clinical trials of porcine islet products in type 1 diabetes—chapter 4: pre-clinical efficacy and complication data required to justify a clinical trial. *Xenotransplantation* 2009;16:229–238
- Hwang Y, Ahn J, Mun J, et al. In vivo analysis of THz wave irradiation induced acute inflammatory response in skin by laser-scanning confocal microscopy. *Opt Express* 2014;22:11465–11475
- Choe K, Jang JY, Park I, et al. Intravital imaging of intestinal lacteals unveils lipid drainage through contractility. *J Clin Invest* 2015;125:4042–4052
- Kim JH, Jin SM, Oh SH, et al. Counting small hypointense spots confounds the quantification of functional islet mass based on islet MRI. *Am J Transplant* 2012;12:1303–1312
- Ricordi C, Lacy PE, Finke EH, Olack BJ, Scharp DW. Automated method for isolation of human pancreatic islets. *Diabetes* 1988;37:413–420
- Andrades P, Asiedu CK, Gansuud B, et al. Pancreatic islet isolation variables in non-human primates (rhesus macaques). *Diabetologia* 2008;51:1236–1244
- Matsumoto S, Takita M, Chaussabel D, et al. Improving efficacy of clinical islet transplantation with iodixanol-based islet purification, thymoglobulin induction, and blockage of IL-1 $\beta$  and TNF- $\alpha$ . *Cell Transplant* 2011;20:1641–1647
- Fennema E, Rivron N, Rouwkema J, van Blitterswijk C, de Boer J. Spheroid culture as a tool for creating 3D complex tissues. *Trends Biotechnol* 2013;31:108–115
- Bartulos O, Zhuang ZW, Huang Y, et al. ISL1 cardiovascular progenitor cells for cardiac repair after myocardial infarction. *JCI Insight* 2016;1:e80920
- von Bahr L, Batsis I, Moll G, et al. Analysis of tissues following mesenchymal stromal cell therapy in humans indicates limited long-term engraftment and no ectopic tissue formation. *Stem Cells* 2012;30:1575–1578
- Qin Z, Schwartzkopff J, Pradera F, et al. A critical requirement of interferon gamma-mediated angiostasis for tumor rejection by CD8+ T cells. *Cancer Res* 2003;63:4095–4100
- Zhong Q, Jenkins J, Moldobaeva A, D'Alessio F, Wagner EM. Effector T cells and ischemia-induced systemic angiogenesis in the lung. *Am J Respir Cell Mol Biol* 2016;54:394–401
- Strand BL, Coron AE, Skjak-Braek G. Current and future perspectives on alginate encapsulated pancreatic islet. *Stem Cells Transl Med* 2017;6:1053–1058
- Jin SM, Oh SH, Oh BJ, et al. Benefits of PEGylation in the early post-transplant period of intraportal islet transplantation as assessed by magnetic resonance imaging of labeled islets. *Islets* 2014;6:e27827
- Haque MR, Jeong JH, Byun Y. Combination strategy of multi-layered surface camouflage using hyperbranched polyethylene glycol and immunosuppressive drugs for the prevention of immune reactions against transplanted porcine islets. *Biomaterials* 2016;84:144–156
- Kim HI, Yu JE, Lee SY, et al. The effect of composite pig islet-human endothelial cell grafts on the instant blood-mediated inflammatory reaction. *Cell Transplant* 2009;18:31–37
- Ho SS, Murphy KC, Binder BY, Vissers CB, Leach JK. Increased survival and function of mesenchymal stem cell spheroids entrapped in instructive alginate hydrogels. *Stem Cells Transl Med* 2016;5:773–781
- Murphy KC, Whitehead J, Falahee PC, Zhou D, Simon SI, Leach JK. Multifactorial experimental design to optimize the anti-inflammatory and proangiogenic potential of mesenchymal stem cell spheroids. *Stem Cells* 2017;35:1493–1504
- Graham ML, Schuurman HJ. The usefulness and limitations of the diabetic macaque model in evaluating long-term porcine islet xenograft survival. *Xenotransplantation* 2013;20:5–17
- Denner J, Graham M. Xenotransplantation of islet cells: what can the non-human primate model bring for the evaluation of efficacy and safety? *Xenotransplantation* 2015;22:231–235